International Journal of Rotating Machinery
1994, Vol. 1, No. 1, pp. 19–35
Reprints available directly from the publisher
Photocopying permitted by license only

On the Development of Two-Dimensional Wakes within Curved Channels: Experimental and Theoretical Investigation

M. T. SCHOBEIRI
Professor, ASME, Turbomachinery Performance Laboratory, Texas A&M University, College Station, TX 77843-3123

K. PAPPU and J. JOHN
Research Assistants

The development of a wake flow downstream of a cylindrical rod within a curved channel under zero streamwise pressure gradient is theoretically and experimentally investigated. The measured asymmetric wake quantities such as the mean velocity and turbulent fluctuations in longitudinal and lateral directions as well as the turbulent shear stress are transformed from the probe coordinate system into the curvilinear wake eigen-coordinate system. For the transformed nondimensionalized velocity defect and the turbulent quantities, affine profiles are observed throughout the flow regime. Based on these observations and using the transformed equations of motion and continuity, a theoretical framework is established that generally describes the two-dimensional curvilinear wake flow. The theory also describes the straight wake as a special case, for which the curvature radius approaches infinity. To demonstrate the general validity of theory, experimental results pertaining to curved wake as well as straight wake flows are compared with the developed theory.

Key Words: *Wake; Cylinder; Curvature; Pressure Gradient; Turbulence*

THE wake flow constitutes a special case of free turbulent flows with a broad range of general scientific and engineering applications. In the field of turbomachinery, the viscous boundary layer flow near the suction and pressure surfaces, in association with the finite blade trailing edge thickness, generates a wake front characterized by strongly asymmetric velocity, Reynolds normal- and shear stress distributions. The wake front moves downstream and influences the boundary layer transition and heat transfer characteristics of the blades positioned downstream of the wake, thus affecting the efficiency and performance of turbomachines.

Earlier experimental and theoretical studies by Reichardt [1950] dealt with free turbulent flows such as the wake flow downstream of blade or cylinder cascades and the free jet flows. From his experimental observations, Reichardt concluded that the defect velocity profiles can statistically be characterized by the error integral functions. Employing an inductive approach, Reichardt established a relationship for the total impulse $\overline{UV}$ as a function of the dimensionless momentum defect. Eifler [1975] and Pfeil and Eifler [1975a, b] extended Reichardt's theory by generating a relationship for the partial impulse $\overline{U}\,\overline{V}$ as a function of the dimensionless momentum and velocity defects. With the above two relations for the total and partial impulses, Pfeil and Eifler [1975] were able to describe the distribution of the turbulent shear stress in x- and y-directions.

The effects of pressure gradient and curvature were investigated by Savill [1983] and recently by Nakayama [1987]. Using a box-shaped test section with one perspex side wall and a metal backplate to deflect a cylinder wake through a right-angle bend, Savill measured the mean velocity profiles and the Reynolds stress components that revealed strong influence of curvature. Nakayama [1987] carried out a systematic study of the effect of mild pres-

sure gradient and mild curvature on a small-defect wake by positioning airfoil-like thin plate at small angles to the external flow. Despite the governing mild pressure and curvature, the turbulence quantities, particularly the shear stress, are strongly affected by the streamline curvature and pressure gradient.

The presented study is part of a comprehensive experimental and theoretical study of the steady and unsteady turbulent wake development through curved channels under positive, zero, and negative longitudinal pressure gradients. An attempt is made to address the basic questions of this type of free turbulent flow by theoretically and experimentally studying the steady wake development in a curved channel under zero-longitudinal pressure gradient.

The theoretical investigations, including the flow model, the corresponding governing equations, and the detail of solution procedures are described in the next section. The sections that follow deal with the description of the experimental setup, data acquisition, reduction, and analysis, and the comparison of analytical and experimental results for the curved as well as straight wake, respectively.

THEORETICAL CONSIDERATIONS

For the following theoretical considerations we assume an incompressible turbulent flow through a two-dimensional curved channel. We further assume that the velocity vector has a temporal and spatial dependency and can be decomposed into a time-independent mean and a time-dependent turbulent fluctuation vector. Based on the experimental observations, the flow regime under investigation can be divided into three distinct zones. First, the wake zone—characterized by strongly asymmetric mean velocity components, turbulent intensities, and shear stress distributions. Second, the wake external zone—where the velocity distribution approximately corresponds to that of a potential flow, even though it is rotational, and thus the assumption of a potential flow character is, strictly speaking, not correct. The third zone is the boundary layer—at the convex and the concave channel walls where the viscosity effect is predominant and the boundary layer approximations can be applied. Based on our own experimental results and in accordance with the investigation of several other researchers, among others, Reichardt [1950], Pfeil and Eifler [1975], Lakshminarayana and Raj [1976], and Nakayama [1987], we further assume that for free turbulent flow, the viscosity effect can practically be neglected. Under these assumptions the conservation equations of fluid mechanics in a coordinate invariant form are treated by transforming from a coordinate invariant form into an orthogonal curvilinear coordinate system by using tensor analytical tools.

Conservation Laws

Before starting with the transformation of conservation laws into curvilinear coordinate system, we decompose the velocity vector into a time-averaged mean and a time-dependent fluctuation as:

$$\vec{V} = \vec{\overline{V}} + \vec{\widetilde{V}} \tag{1}$$

Using the above decomposition, the corresponding index notation for the two-dimensional orthogonal curvilinear coordinate system, the continuity and momentum equations in time-averaged sense can be written as:

$$\overline{V}^i_{,i} + \overline{V}^i \Gamma^j_{ij} = 0 \tag{2}$$

$$\begin{aligned} &\overline{V}^j \overline{V}^i_{,j} + \overline{V}^j \overline{V}^k \Gamma^i_{kj} \\ &= -\frac{1}{\rho} g^{ij} \overline{p}_{,j} - (\overline{\widetilde{V}^m \widetilde{V}^i})_{,m} - \overline{\widetilde{V}^m \widetilde{V}^i} \Gamma^j_{mj} \\ &\quad - \overline{\widetilde{V}^m \widetilde{V}^n} \Gamma^i_{mn} \end{aligned} \tag{3}$$

$$\begin{aligned} &(\overline{V}^m \overline{V}^j)_{,m} + \overline{V}^m \overline{V}^j \Gamma^i_{mi} + \overline{V}^m \overline{V}^n \Gamma^j_{mn} \\ &= -\frac{1}{\rho} g^{ji} \overline{p}_{,i} - (\overline{\widetilde{V}^m \widetilde{V}^j})_{,m} - \overline{\widetilde{V}^m \widetilde{V}^j} \Gamma^i_{mi} \\ &\quad + \overline{\widetilde{V}^m \widetilde{V}^n} \Gamma^j_{mn} \end{aligned} \tag{4}$$

Inserting the metric coefficients and Christoffel symbols:

$$g_{ij} = \begin{pmatrix} \left(\frac{R+\xi_2}{R}\right)^2 & 0 \\ 0 & 1 \end{pmatrix};$$

$$g^{ij} = \begin{pmatrix} \left(\frac{R}{R+\xi_2}\right)^2 & 0 \\ 0 & 1 \end{pmatrix} \tag{5}$$

$$\Gamma^1_{ij} = \begin{pmatrix} 0 & \left(\frac{1}{R+\xi_2}\right) \\ \left(\frac{1}{R+\xi_2}\right) & 0 \end{pmatrix};$$

$$\Gamma^2_{ij} = \begin{pmatrix} -\left(\frac{R+\xi_2}{R^2}\right) & 0 \\ 0 & 1 \end{pmatrix} \tag{6}$$

and introducing $\overline{U}$ and $\overline{V}$ for the time-averaged physical components of V^i and $\overline{u^2}$, $\overline{v^2}$, $\overline{uv}$ for the time-averaged physical components of fluctuation impulse $\overline{\tilde{V}^i\tilde{V}^j}$, time-averaged version of the continuity equation (Eq. [2]) is written as:

$$\overline{U}_{,1} + \left[\left(1 + \frac{\xi_2}{R}\right)\overline{V}\right]_{,2} = 0 \tag{7}$$

Eq. [3] is decomposed in longitudinal direction ξ_1:

$$\frac{R}{R+\xi_2}\overline{U}\,\overline{U}_{,1} + \overline{V}\,\overline{U}_{,2} + \frac{\overline{U}\,\overline{V}}{R+\xi_2} = -\frac{1}{\rho}\frac{R}{R+\xi_2}\overline{p}_{,1} - \frac{R}{R+\xi_2}(\overline{u^2})_{,1} - (\overline{uv})_{,2} - \frac{2}{R+\xi_2}\overline{uv} \tag{8}$$

and lateral direction ξ_2:

$$\frac{R}{R+\xi_2}\overline{U}\,\overline{V}_{,1} + \overline{V}\,\overline{V}_{,2} - \frac{\overline{U}^2}{R+\xi_2} = -\frac{1}{\rho}\overline{p}_{,2} - \frac{R}{R+\xi_2}(\overline{uv})_{,1} - (\overline{v^2})_{,2} - \frac{\overline{v^2}}{R+\xi_2} + \frac{\overline{u^2}}{R+\xi_2} \tag{9}$$

Similarly Eq. [4], decomposed into ξ_1, ξ_2 components is written as:

$$\frac{R}{R+\xi_2}\left(\frac{\overline{p}}{\rho} + \overline{U}^2 + \overline{u^2}\right)_{,1} + (\overline{U}\,\overline{V} + \overline{uv})_{,2} + \frac{2}{R+\xi_2}(\overline{U}\,\overline{V} + \overline{uv}) = 0 \tag{10}$$

$$\frac{R}{R+\xi_2}(\overline{U}\,\overline{V} + \overline{uv})_{,1} + \left(\frac{\overline{p}}{\rho} + \overline{V}^2 + \overline{v^2}\right)_{,2} - \frac{1}{R+\xi_2}\left(\overline{U}^2 - \overline{V}^2 + \overline{u^2} - \overline{v^2}\right) = 0 \tag{11}$$

Eqs. [10] and [11] are of practical interest for estimating the order of magnitude of each individual term compared with the others. For the special case of zero longitudinal pressure gradient, presented in this paper, the changes in static pressure in longitudinal direction is set equal to zero. Furthermore, as the experimental results show, the longitudinal fluctuation velocity $|u|$ is considerably smaller than the mean velocity $\overline{U}$. The lateral fluctuation velocity $|v|$, however, has the same order of magnitude as the mean lateral velocity $\overline{V}$, while it is negligible compared to $\overline{U}$. This comparison leads to the conclusion that the contributions of the fluctuation velocity momenta are negligibly small compared with the contribution of the longitudinal mean velocity momentum $\overline{U}^2$. However, it should be pointed out that the above-mentioned contributions are not neglected in this investigation.

Nondimensional Wake Parameters

Eqs. [7], [10], and [11] describe the wake development phenomenon through a curved channel. To solve these equations for the required wake characteristics we assume that from a definite distance downstream of the wake origin the velocity as well as the momentum defect profiles are similar. This assumption implies that for arbitrary points located on the wake center with the longitudinal coordinate ξ_1, corresponding length scale $b = b(\xi_1)$ on the lateral coordinate ξ_2 can be found to generate the dimensionless variable:

$$\zeta = \frac{\xi_2}{b} \text{ with } b = \frac{1}{2\Gamma}\int_{-\infty}^{+\infty}\frac{\overline{U}_1}{\overline{U}_{1m}}d\xi_2 \text{ and}$$

$$\Gamma = \int_0^{\infty} e^{-\zeta^2}d\zeta = 0.886 \tag{12}$$

Furthermore, the wake velocity and momentum defects are defined as:

$$\overline{U} = U_p - \overline{U}_1 \tag{13}$$

$$\overline{U}^2 = U_p^2 - \overline{U}_I^2 \text{ with } \overline{U}_I^2 = 2U_p\overline{U}_1 - \overline{U}_1^2 \tag{14}$$

In Eq. [13], U_p represents the hypothetical velocity distribution which is an extension of the undisturbed wake-external velocity into the wake. In the vicinity of the wake center, it can be shown by employing the equation of motion [Eq. 8] for potential flow that the velocity U_p can be approximated as:

$$U_p = U_{p0}\left(1 - \frac{\xi_2}{R}\right) \tag{15}$$

with U_{p0} as the hypothetical velocity at the wake center, $\xi_2 = 0$. Thus for the zero pressure gradient case presented in this paper, U_p is a function of ξ_2 only. The time-averaged velocity and momentum defects within the wake region are represented by $\overline{U}_1$ and $\overline{U}_I^2$.

The similarity assumption, stated previously, requires the following dimensionless wake velocity as well as the

momentum defect functions:

$$\varphi_1 = \frac{\overline{U}_1}{\overline{U}_{1m}}, \quad \varphi^2 = \frac{\overline{U}_I^2}{\overline{U}_{Im}^2} \tag{16}$$

Here $\overline{U}_{1m}$, $\overline{U}_{Im}^2$ represent the maximum wake velocity and momentum defects at the wake center.

Expressions for Wake Characteristics

Introducing the wake velocity defect Eq. [16] in connection with Eq. [13] into continuity equation [7], separating the variables and integrating the resulting equation, we obtain:

$$\left(1+\frac{\xi_2}{R}\right)\overline{V} = -\int \frac{d}{d\xi_1}\left[U_{p0}\left(1-\frac{\xi_2}{R}\right) - \overline{U}_{1m}\varphi_1\right] b d\zeta + c \tag{17}$$

After some rearrangement of terms, Eq. [17] leads to:

$$\left(1+\frac{\xi_2}{R}\right)\overline{V} = \frac{d(\overline{U}_{1m}b)}{d\xi_1}\int \varphi_1 d\zeta - \frac{db}{d\xi_1}\overline{U}_{1m}\varphi_1\zeta - \frac{dU_{p0}}{d\xi_1} b \int \left(1-\frac{\zeta b}{R}\right) d\zeta + c \tag{18}$$

Eq. [18] shows that the lateral velocity is determined by the turbulent mixing and the decay process in longitudinal direction characterized by the longitudinal changes of the velocity-width product $\overline{U}_{1m}b$. Experimental investigations by Reichardt [1950], Eifler [1975], Pfeil and Eifler [1975], and our own measurements show that for the wake development downstream of a single cylinder under zero streamwise pressure gradient this product is approximately constant. However, for positive respectively negative streamwise pressure gradients it was found that the product $\overline{U}_{1m}b$ exhibits a pronounced dependency in longitudinal direction ξ_1. Also for the case of zero longitudinal pressure gradient, the variations in U_{p0} with streamwise distance can be neglected. Since the lateral velocity component $\overline{V}$ is zero at the wake center, the integration constant in Eq. [18] must identically vanish. Implementing the above approximations, Eq. [18] simplifies to:

$$\overline{V} = -\frac{R}{R+\xi_2}\frac{db}{d\xi_1}\overline{U}_{1m}\varphi_1\zeta \tag{19}$$

With Eq. [19] the distribution of the lateral velocity component can be found provided the wake velocity defect function φ_1, the distribution of the wake width $b = b(\xi_1)$ as well as the distribution of $\overline{U}_{1m}$ are known.

From the assumption of similarity in wake velocity defect profiles, it follows that for an appropriately chosen length and velocity scale, wake width and maximum wake velocity defect in this case, nondimensional wake velocity defect will be a function of $\zeta = \xi_2/b$ only, that is:

$$\frac{\overline{U}_1}{\overline{U}_{1m}} = f\left(\frac{\xi_2}{b}\right) = f(\zeta) \tag{20}$$

From the experimental investigations by Reichardt [1950], Eifler [1975], and others it was concluded that the nondimensional wake velocity defect distribution in case of a straight channel with zero streamwise pressure gradient follows the Gaussian distribution. Similar solution for the dimensionless wake velocity defect function, in Eq. [20], in case of curved channel wake flow can be obtained by using equation of motion (Eq. [8]) with earlier specified order of magnitude analysis. The derivation involves the use of the expressions for mean longitudinal and lateral velocities, i.e., Eqs. [13] and [19], and also of shear stress. The analytical treatment with suitable approximations results in an ordinary second order differential equation in φ_1, the numerical solution of which is found to follow the Gaussian distribution presented below.

$$\varphi_1 = e^{-\zeta^2} \tag{21}$$

Comprehensive experimental measurements in curved channels with and without streamwise pressure gradient are also found to follow the Gaussian distribution given by Eq. [21] as well, indicating the validity of similarity assumption in wake velocity defect profiles.

From the time-averaging procedure, it is obvious that shear stress is the difference of total and partial impulses, i.e, $\overline{uv} = \overline{U}\,\overline{V} - \overline{U}\,\overline{V}$. Using the expressions for mean velocities from Eqs. [13] and [19], the expression for partial impulse can be written as:

$$\overline{U}\,\overline{V} = -(U_p - \overline{U}_{1m}\varphi_1)\overline{U}_{1m}\frac{db}{d\xi_1}\zeta\varphi_1\frac{R}{R+\xi_2} \tag{22}$$

Substituting the approximation for U_p from Eq. [15] into Eq. [22] and nondimensionalizing the resulting equation with $\overline{U}_{1m}^2$, final expression for nondimensional partial impulse is written as:

$$\frac{\overline{U}\,\overline{V}}{\overline{U}_{1m}^2} = -\frac{R}{R+\xi_2}\frac{db}{d\xi_1}\frac{U_{p0}}{\overline{U}_{1m}}\left(1-\frac{\zeta b}{R}\right)\zeta\varphi_1 + \frac{R}{R+\xi_2}\frac{db}{d\xi_1}\zeta\varphi_1^2 \tag{23}$$

The expression for total impulse can be obtained by using the equation of motion (Eq. [10]) in ξ_1 direction and following the earlier specified order of magnitude analysis as:

$$\frac{R}{R+\xi_2}(\overline{U}^2+\overline{u^2})_{,1}+(\overline{UV})_{,2}+\frac{2}{R+\xi_2}(\overline{UV}) = -\frac{1}{\rho}\frac{R}{R+\xi_2}\overline{P}_{,1} \quad (24)$$

Assuming that the longitudinal turbulent intensity is negligible in comparison with the mean velocity of the flow, also the variation of the potential velocity at the wake center in ξ_1 direction is very small for the case of zero longitudinal pressure gradient, Eq. [24] in connection with Eqs. [13] and [14] can be simplified as:

$$\frac{R}{R+\xi_2}\frac{\partial}{\partial\xi_1}\left(-\overline{U}_I^2\right) = -(\overline{UV})_{,2}-\frac{2}{R+\xi_2}(\overline{UV}) \quad (25)$$

Further rearrangement of terms, the assumption $\frac{\overline{UV}}{R} \ll \frac{\partial}{\partial\xi_2}[(1+\frac{\xi_2}{R})(\overline{UV})]$, and integration of the resulting equation yield an expression for total impulse as:

$$\left(1+\frac{\xi_2}{R}\right)(\overline{UV}) = \int\frac{d}{d\xi_1}(\overline{U}_I^2)b\,d\zeta + c = \int\frac{d}{d\xi_1}(\overline{U}_{Im}^2\varphi^2)b\,d\zeta + c \quad (26)$$

where $\overline{U}_{Im}^2 = 2U_p\overline{U}_{1m}-\overline{U}_{1m}^2$.

The approximate equality of dimensionless wake velocity and momentum defects, i.e., $\varphi^2 \cong \varphi_1$, has been verified experimentally for different locations downstream of the wake generating body. Using this approximation and further rearrangement of some terms modify Eq. [26] to:

$$\left(1+\frac{\xi_2}{R}\right)\overline{UV} = \int\left(-2U_p\overline{U}_{1m}\frac{db}{d\xi_1}+\overline{U}_{1m}^2\frac{db}{d\xi_1}\right)\times\frac{d}{d\zeta}(\zeta\varphi_1)d\zeta + \int 2\overline{U}_{1m}b\left(1-\frac{\xi_2}{R}\right)\varphi_1\times\frac{dU_{p0}}{d\xi_1}d\zeta + \int 2U_p\varphi_1\frac{d}{d\xi_1}(\overline{U}_{1m}b)d\zeta - \int\varphi_1\times\frac{d}{d\xi_1}(\overline{U}_{1m}^2b)d\zeta + c \quad (27)$$

The above equation can further be simplified as $\overline{U}_{1m}b$ is constant and the changes in U_{p0} in ξ_1 direction are quite small for zero longitudinal pressure gradient case. The simplification, evaluation of the integrals, and finally nondimensionalizing with $\overline{U}_{1m}^2$ result in an expression for total impulse as:

$$\frac{\overline{UV}}{\overline{U}_{1m}^2} = \frac{R}{R+\xi_2}\frac{U_{p0}}{\overline{U}_{1m}}\frac{db}{d\xi_1}\left[-2\zeta\varphi_1+\frac{b\varphi_1}{R}(1+2\zeta^2)\right] + \frac{R}{R+\xi_2}\frac{db}{d\xi_1}\zeta\varphi_1+\frac{c}{\overline{U}_{1m}^2} \quad (28)$$

Now the expression for Reynolds shear stress can be obtained from the difference of total impulse and partial impulse, i.e, Eqs. [23] and [28], as:

$$\frac{\overline{uv}}{\overline{U}_{1m}^2} = \frac{R}{R+\xi_2}\frac{U_{p0}}{\overline{U}_{1m}}\frac{db}{d\xi_1}\left[-\zeta\varphi_1+\frac{b\varphi_1}{R}(1+\zeta^2)\right] + \frac{R}{R+\xi_2}\frac{db}{d\xi_1}\zeta\varphi_1(1-\varphi_1)+\frac{c}{\overline{U}_{1m}^2} \quad (29)$$

The constant of integration in the above expression is a function of ξ_1 and needs to be evaluated from the experimental results at $\zeta = 0$. For the case of straight channel with no streamwise pressure gradient, it is known from experimental results that shear stress is zero at the wake center with the distribution being symmetric about the wake center. In that case, the constant of integration evaluates to be zero. But for the case of curved channel flow, the shear stress distribution is strongly asymmetric with the value of it being non-zero at the wake center, thus bringing out the influence of curvature. As a result, the constant of integration is no longer zero and needs to be evaluated from experimental measurements to incorporate the asymmetry.

EXPERIMENTAL RESEARCH FACILITY

The experimental facility described here enables the simulation of steady and unsteady wake development in a two-dimensional curved channel with positive, zero, and negative longitudinal pressure gradients. The wake is generated by a circular cylinder. The use of cylinder instead of blade cascade is appropriate, since the turbulence characteristics of the cylinder wake flows, in terms of Reynolds stress components, are similar to those of rotor blade wakes.

The test facility shown in Fig. 1 consists of a large centrifugal fan, a settling chamber, a nozzle, a wake generator, a test section, and an exit duct. For detailed information about the design description and performance tests

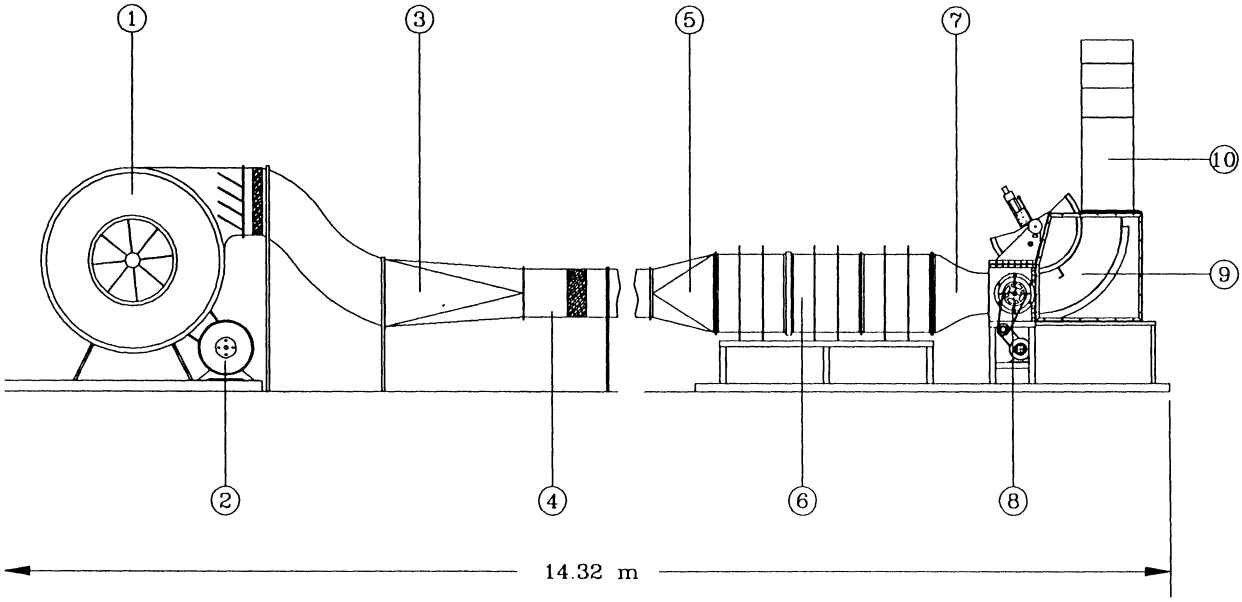

FIGURE 1 Overall layout of the test facility: 1—fan; 2—motor; 3—transition duct; 4—straight pipe; 5—diffuser; 6—settling chamber; 7—nozzle; 8—wake generator; 9—test section; 10—exit duct.

we refer to a report and a paper by Schobeiri [1988] and Schobeiri and Pardivala [1992].

The test section shown in Fig. 2 is located downstream of the wake generator and consists of a convex top wall, a concave bottom wall, and two vertical plexiglass side walls. The probe traversing system is mounted within the convex wall assembly, details of which are discussed in the following section. The concave bottom wall is designed to slide horizontally within two T-slots in the bottom wall of the wake generator. This allows the creation of adverse or favorable longitudinal pressure gradients within the test section. The two curved walls have static pressure ports mounted flush with the surface at regular arc lengths of 50 mm. The static pressure ports are connected to a manometer bank for visualization purposes. The test section allows the integration of test objects such as a curved plate, a cylinder, or a turbine cascade for boundary layer and heat transfer investigations.

In addition to simulating convex curvature, the convex wall assembly is designed to allow precise radial and circumferential traversing of the probes. Figure 2 shows the mounting of the traversing system within the convex wall assembly. The traversing system is mounted vertically on the base plate of the convex wall assembly. It consists of a 152.4 mm slider that moves within a dovetail guide. A lead screw, with a maximum traversing length of 610.0 mm, is connected to a DC stepper motor to provide the required drive for the slider. It receives signals from a computer and is driven by a FORTRAN code, with an arbitrary traversing schedule as an input, and turns the lead screw by the exact number of pulses required. An optical encoder connected to the traversing system provides a continuous feedback to the stepper motor for accurate positioning of the probes. The system is capable of traversing in small steps with a minimum of 2.5 μm, which is specifically required for boundary layer investigations, where the measurement of the laminar sublayer is of particular interest. Software stops and mechanical stops are used to prevent the probes from traversing beyond the desired limits.

The slider of the traversing system is designed to allow the simultaneous positioning of two probes. The first probe is a hot-film X-probe, while the second probe is a pneumatic probe (Kiel probe). Angular positioning of the probes is achieved by rotating the entire convex wall assembly about its center of curvature. A rotary vernier is mounted on one of the triangular supporting walls for precise angular positioning of the probes.

INSTRUMENTATION, DATA ACQUISITION, AND DATA REDUCTION

The mean velocity and turbulent stress components are obtained using a 3-channel, constant temperature anemometer (TSI, IFA 100) system. Based on numerous spectral measurements within the wake, the low-pass filter of the signal conditioner is set at 20 kHz. All the measurements

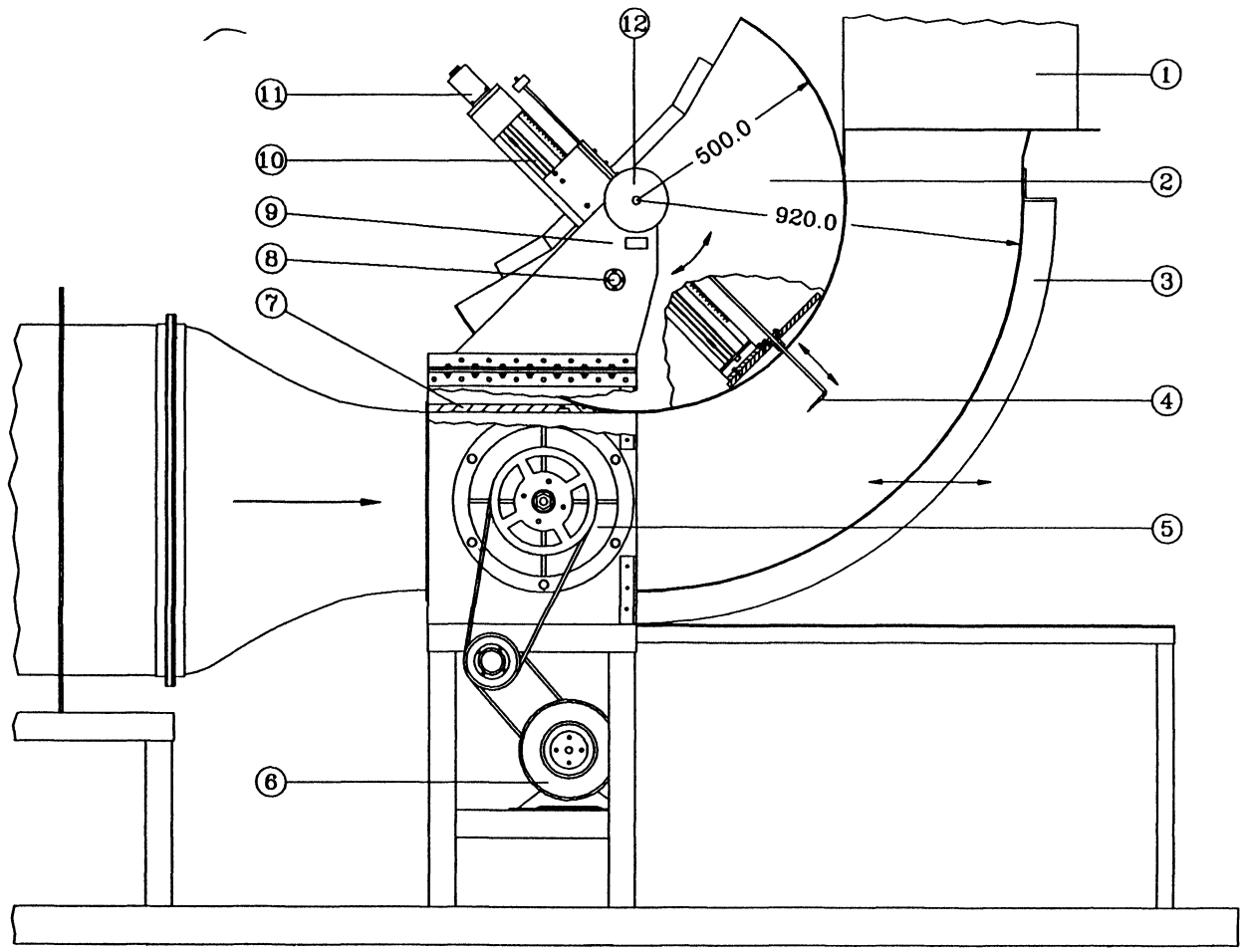

FIGURE 2 Test section: 1—exit duct; 2—convex wall assembely; 3—concave wall; 4—probe; 5—wake generag; 6—motor; 7—top wall; 8—saftey pin; 9—rotary vernier; 10—traversing system; 11—stepper motor; 12—locking wheel.

in the present study are made with platinum hot-film sensors of 25 μm in diameter. The X-film probe is designed to allow the sensors to remain along the axis of the probe support. The first channel of the anemometer is connected to a single-film probe and the second and third channels are connected to a X-film probe. The fourth and fifth channels of the A/D board are connected with two high-precision differential pressure transducers (MKS 220CD, Range: 0–10 mm Hg and 0–100 mm Hg) with a 2-channel digital readout. The pressure transducers are of capacitance type and have 0–10 V analog outputs. A Prandtl probe (pitot-static probe), placed upstream of the diffuser, is connected to one of the pressure transducers to monitor the reference velocity at a fixed location. The second pressure transducer is used to measure the total pressure from a Kiel probe positioned at the same radial and longitudinal location as the X-probe.

In order to ensure a high level of accuracy and accelerate the calibration procedure, the simple calibration method by John and Schobeiri [1993] was used. For the data reduction and analysis, the characteristic response of X-film probe is stored in the form of calibration coefficients. The velocity components are obtained in the probe coordinates which in the present measurements coincide with the radial and tangential directions to the convex wall. The instantaneous velocity component in tangential direction is denoted by V_x and in the radial direction is denoted by V_y. The radial velocity V_y is taken positive if its direction is toward the convex wall. The instantaneous velocity components can be represented in the following form.

$$V_x = \overline{V}_x + v_x; \quad V_y = \overline{V}_y + v_y \tag{30}$$

$\overline{V}_x$ and $\overline{V}_y$ are the mean (time-averaged) velocity components in x and y directions (tangential and radial directions), respectively. The turbulent fluctuation components

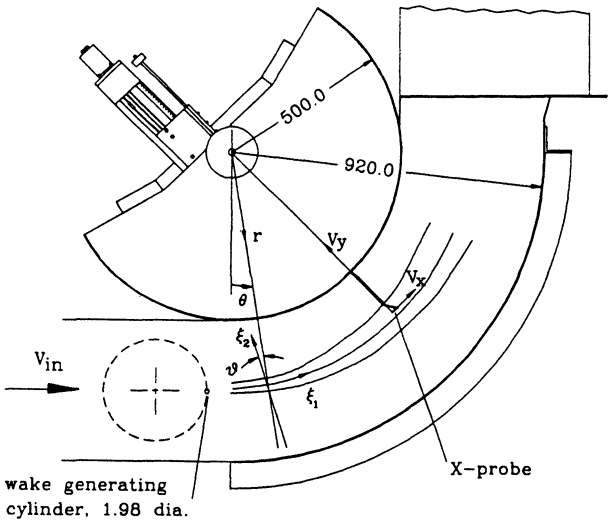

FIGURE 3 Representation of probe coordinate and the wake eigencoordinate systems.

are denoted by v_x and v_y. The mean velocity components, also known as time average or global mean, are given by

$$\overline{V}_x = \frac{1}{N}\sum_{j=1}^{N} V_{x_j}, \tag{31}$$

$$\overline{V}_y = \frac{1}{N}\sum_{j=1}^{N} V_{y_j} \tag{32}$$

where $N(= 32{,}768)$ is the total number of samples per sensor of the X-film probe at one probe location. At the sampling rate of 2 kHz, employed in the investigation of steady wakes, 32,768 samples per sensor provided good convergence for the mean velocities and Reynolds stresses. The mean square values of the components of turbulent velocity fluctuations are obtained from the instantaneous and mean velocities as

$$\overline{v_x^2} = \frac{1}{N}\sum_{j=1}^{N}\left(V_{x_j} - \overline{V}_x\right)^2 \tag{33}$$

$$\overline{v_y^2} = \frac{1}{N}\sum_{j=1}^{N}\left(V_{y_j} - \overline{V}_y\right)^2 \tag{34}$$

The Reynolds shear stress is calculated by

$$\overline{v_x v_y} = \frac{1}{N}\sum_{j=1}^{N}\left(V_{x_j} - \overline{V}_x\right)\left(V_{y_j} - \overline{V}_y\right) \tag{35}$$

The measurements are made in the probe coordinates (x, y), shown in Fig. 3, giving the tangential velocity component $\overline{V}_x$ and radial velocity component $\overline{V}_y$. In order to compare experimental results with the theory developed previously, the results have to be represented in a curvilinear coordinate system $(\xi_1$–$\xi_2)$. In accordance with the definitions used earlier, ξ_1 is defined as the direction along a streamline near the center of wake and ξ_2 the direction normal to it. The maximum inclination between these two orthogonal coordinate systems was found to be less than 7.5° for the data presented here, and hence, the distance taken radially from the wake center to a measuring point was approximated as ξ_2 and for all the measuring points at an angular position θ, the ξ_1 coordinate was assumed constant. The errors due to this approximation will be even small considering the fact that for most longitudinal locations the inclination between the two coordinate systems was less than 4°.

The equations for transforming the time-averaged velocity and turbulent stresses calculated in the (x, y)-coordinate to the curvilinear coordinate system $(\xi_1$–$\xi_2)$ are given by Eqs. [38]–[42]. The instantaneous velocity components in the $(\xi_1$–$\xi_2)$ can be represented by the instantaneous velocity components in (x, y)-coordinates.

$$U = V_x \cos\vartheta + V_y \sin\vartheta \tag{36}$$

$$V = V_y \cos\vartheta - V_x \sin\vartheta \tag{37}$$

where ϑ is the angle between the ξ_1 and x-direction. Also, the mean velocity components in $(\xi_1$–$\xi_2)$ is obtained from mean velocities in the (x, y)-coordinates by:

$$\overline{U} = \overline{V}_x \cos\vartheta + \overline{V}_y \sin\vartheta \tag{38}$$

$$\overline{V} = \overline{V}_y \cos\vartheta - \overline{V}_x \sin\vartheta \tag{39}$$

where $\overline{U}$ and $\overline{V}$ are the mean velocities in ξ_1 and ξ_2 directions, respectively. Subtracting the value of mean velocity from the instantaneous one gives the fluctuating velocity $(u = U—\overline{U}, v_x = V_x - \overline{V}_x$, etc.). The mean Reynolds stress components in $(\xi_1$–$\xi_2)$-coordinates are obtained by taking the product of the fluctuating velocities and time averaging, and are given by:

$$\overline{u^2} = \overline{v_x^2}\cos^2\vartheta + \overline{v_y^2}\sin^2\vartheta + \overline{v_x v_y}\sin 2\vartheta \tag{40}$$

$$\overline{v^2} = \overline{v_x^2}\sin^2\vartheta - \overline{v_y^2}\cos^2\vartheta - \overline{v_x v_y}\sin 2\vartheta \tag{41}$$

$$\overline{uv} = \left(\overline{v_y^2} - \overline{v_x^2}\right)\frac{\sin 2\vartheta}{2} + \overline{v_x v_y}\cos 2\vartheta \tag{42}$$

The velocity defect distribution is determined from the wake velocity data and hypothetical potential velocity distribution. In order to obtain the location of maximum velocity defect accurately, a smoothing cubic spline function

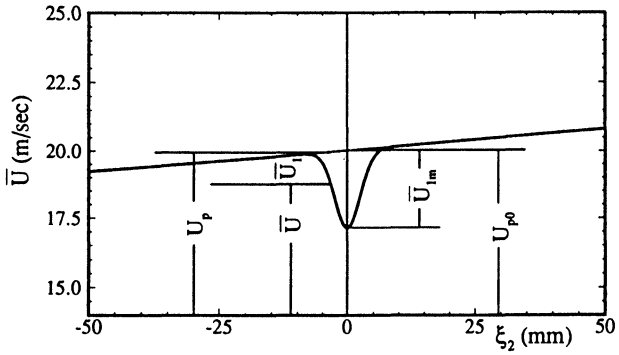

FIGURE 4 Nondimensional parameters.

is used to fit the tangential component of velocity defect, $\overline{V}_{x1}$ ($\overline{V}_{x1} = \overline{V}_{xp} - \overline{V}_x$). The edges of the wake were determined by an integral method developed by Schobeiri et al. [1992]. The location of wake edges are sensitive to the initial selection of the potential region used to determine the hypothetical potential velocity distribution. However, the integral parameters such as wake width are much less sensitive to the location of wake edges, especially if the location of the wake edges are in the potential flow region.

The components of mean velocity and Reynolds stresses in curvilinear coordinate system are calculated from Eqs. [38]–[42]. The velocity defect distribution, maximum value of velocity defect, and the location of maximum velocity defect are calculated for the longitudinal component $\overline{U}$. Figure 4 shows the schematic diagram of the velocity defect distribution for the longitudinal velocity.

RESULTS AND DISCUSSION

The validity of theory developed in the Theoretical Considerations section is accomplished by comparing it with the experimental results available from curved channel, discussed previously, and also from literature. To carry out the comparison with theory, information regarding the wake width, maximum wake velocity defect, and hypothetical potential flow velocity at the wake center are taken from the experimental measurements.

Curved Channel Wake Flow

Wake development. The wake behind a stationary cylinder with the diameter $d = 1.984$ mm located at mid-height of the wake generating section, was measured using a X-hot-film probe. The curved channel test section had an inlet to exit area ratio of 1 and an average inlet velocity of 20 m/s. The wake profiles were obtained at fifteen angular positions (also referred to as longitudinal positions) from $\theta = 0°$ to 70° in 5° intervals. The first measuring station $\theta = 0°$ corresponds to the inlet of the curved test section, and is at a distance of 67 mm downstream of the wake generating cylinder. Based on the results of theoretical and experimental investigations on straight wake, presented in the next section, it was found unnecessary to vary the cylinder diameter as a parameter for curved wake.

The wake center is defined as the location of maximum velocity defect, as shown in Fig. 4. The path of wake center represents the direction of curvilinear coordinate ξ_1 at $\xi_2 = 0$. As the wake propagates through the channel, the trajectory of the wake center gradually moves toward the convex wall up to a longitudinal location $\xi_1/d = 240$, and from there onward it moves away from the convex wall. The maximum inclination between the trajectory of the wake center and the tangential direction x was less than 5°. The maximum velocity defect and the potential velocity are sketched in Fig. 4.

The decay of the maximum velocity defect $\overline{U}_{1m}$ normalized by the potential velocity at the wake center U_{p0} is shown in Fig. 5(a). The solid line represents a power law fit with $\overline{U}_{1m}/U_{p0} \sim (\xi_1/d)^m$. The experimental results suggest that the exponent m is, among others, a function of pressure gradient and may assume different values. In the present study m can be approximated as $m = -0.71$. For comparison, the straight wake decay process follows the relationship $\overline{U}_{1m}/U_\infty \sim (x/d)^{-0.5}$ for near wake ($x/d < 100$) and $\overline{U}_{1m}/U_\infty \sim (x/d + x_0/d)^{-0.5}$ for far wake ($x/d > 100$) (see Reichardt [1950]; Pfeil and Eifler [1975]). The value of the virtual origin x_o reported by different researchers varies from 40 to $100d$. It is evident that the decay of wake centerline velocity defect for the present curved wake is faster than the straight wake. This is mainly due to the asymmetric character of wake velocity distribution mentioned above.

The wake growth characterized by b/d as a function of ξ_1/d is shown in Fig. 5(b), the solid line being the power law fit with $b/d \sim (\xi_1/d)^m$ with the exponent m being equal to 0.74. For comparison, for a zero-pressure gradient straight wake b/d is proportional to $(x/d)^{0.5}$ for near wake and $(x/d + x_o/d)^{0.5}$ for far wake. This results in a higher growth rate b for curved wake compared to that of the straight wake. Considering the relationships for $\overline{U}_{1m}$ and b/d, the product $\overline{U}_{1m}b$ leads to almost a constant value, which is characteristic for turbulent wake flow at zero pressure gradient.

Mean velocity distribution. The distribution of the mean velocity defect function $\varphi_1 = \overline{U}_1/\overline{U}_{1m} = f(\zeta)$ for different longitudinal locations is shown in Fig. 6. The lat-

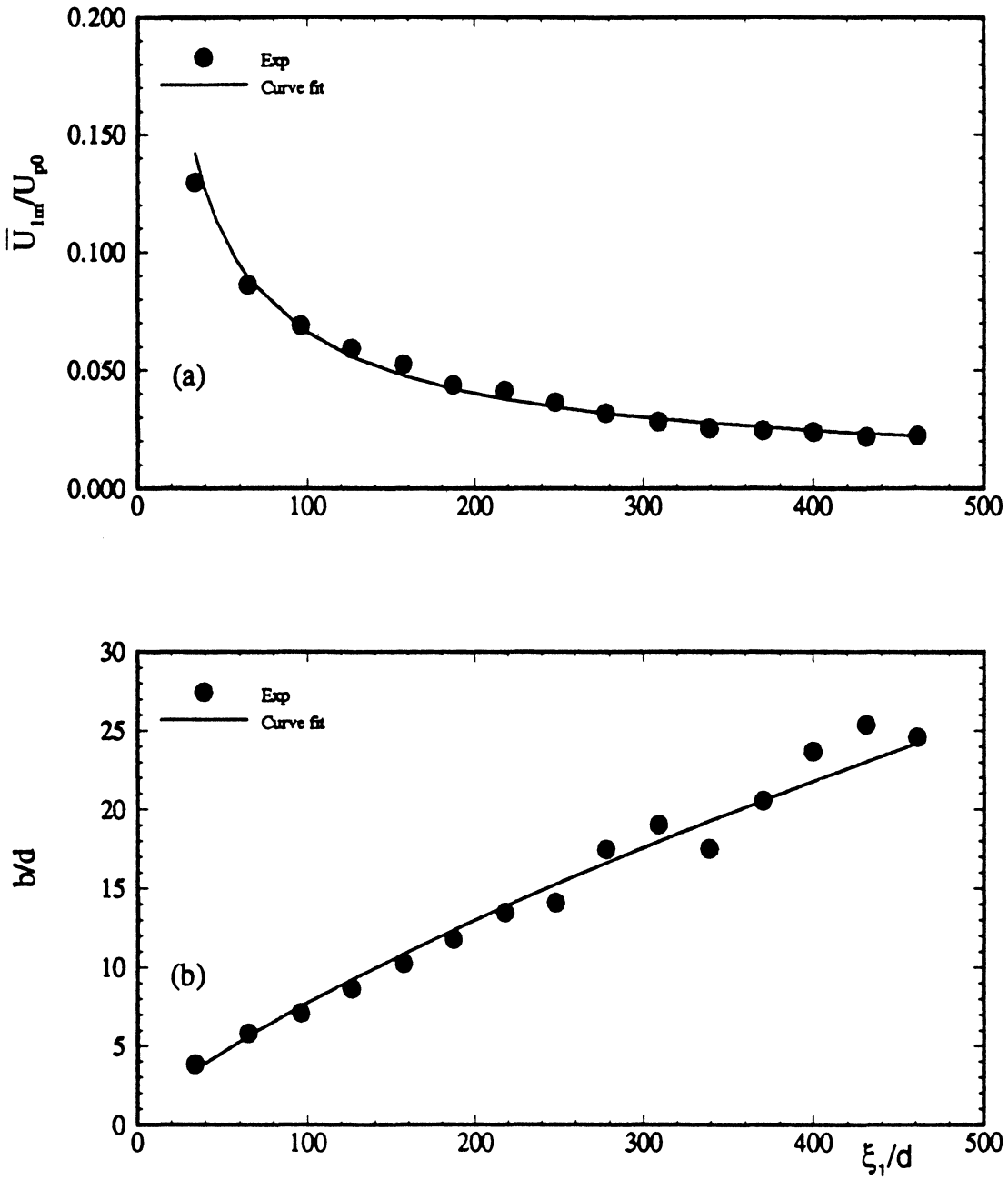

FIGURE 5 Nondimensionalized (a) maximum velocity defect; and (b) wake width as a function of ξ/d.

eral distance ξ_2 is nondimensionalized by the wake width b. Considering the asymmetric behavior of the velocity distribution, the introduction of the velocity defect has resulted in a fully symmetric defect function.

In Fig. 6 the experimental results (symbols) are compared with the theory (solid line) developed in Theoretical Considerations. The solid lines are based on the velocity defect function, $\varphi_1 = e^{-\zeta^2}$, which is proved to be a general representation of the wake defect for curved and straight wakes (see the next section). The mean velocity defect profiles are symmetric and almost identical to the straight wake (discussed in the next section) except for the fact that they are slightly wider on the inner side (concave side of the trajectory of the wake centerline) of the wake. This small deviation from the straight wake data is more clear at higher longitudinal locations. In general, it may be con-

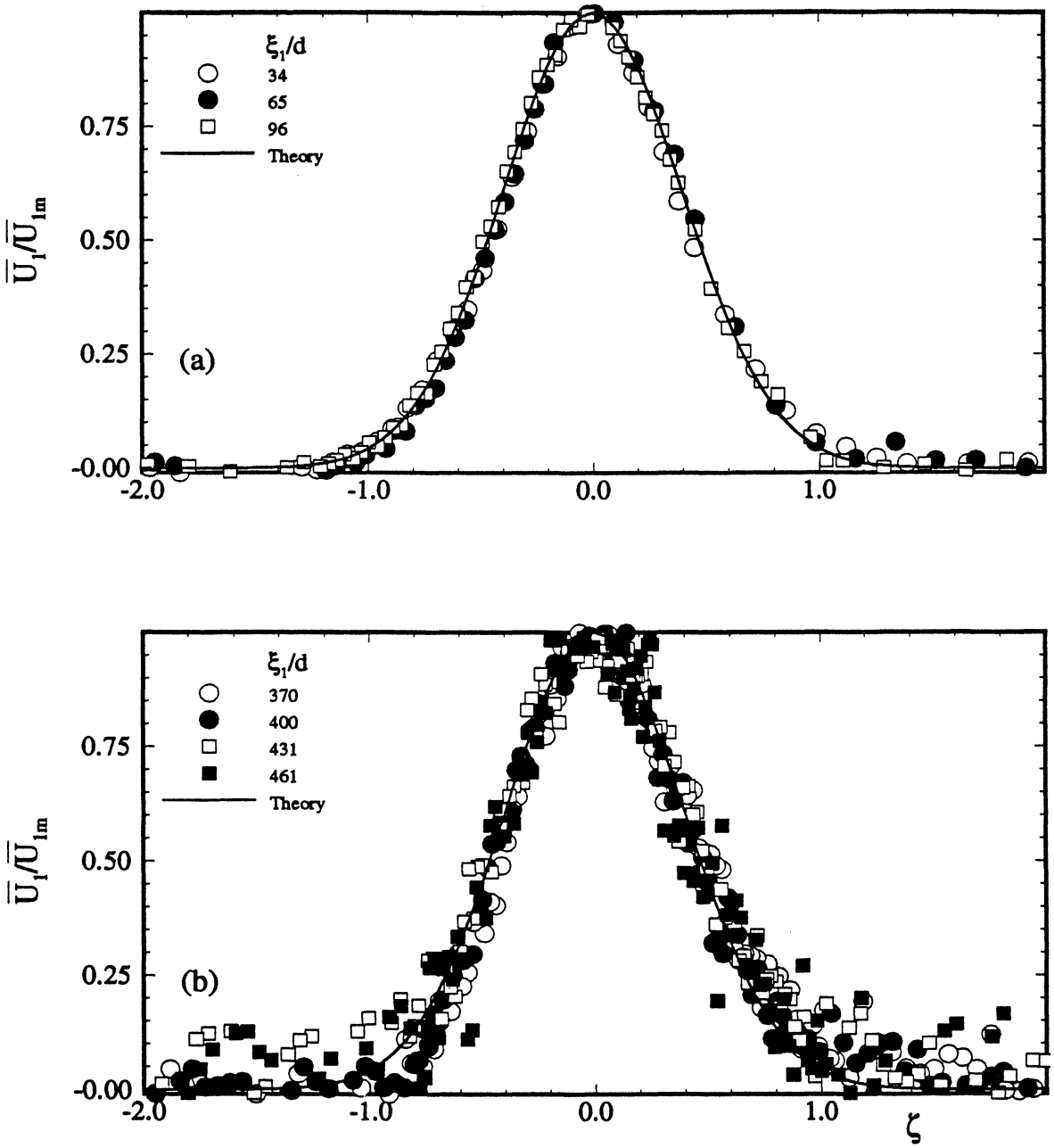

FIGURE 6 Mean defect velocity distribution in curved channel, comparision of theory (solid lines) and experiment (symbols).

sidered that the effect of curvature on mean velocity defect distribution is small. The higher scatter of the normalized velocity defect at higher downstream locations is due to the fact that the maximum velocity defect is very small at these locations.

The distribution of the experimental and theoretical mean longitudinal velocity components are shown for different longitudinal locations in Fig. 7, where experimental and theoretical results are represented by symbols and lines respectively. As shown, the velocity distribution exhibits a strong asymmetric character with higher velocities at the positive side of ξ_2, corresponding to the locations closer to the convex wall with $\xi_2 = 0$ as the geometric location of the wake center. The wake velocity defect decreases resulting in a continuous increase of the wake width with downstream location. The individual velocity

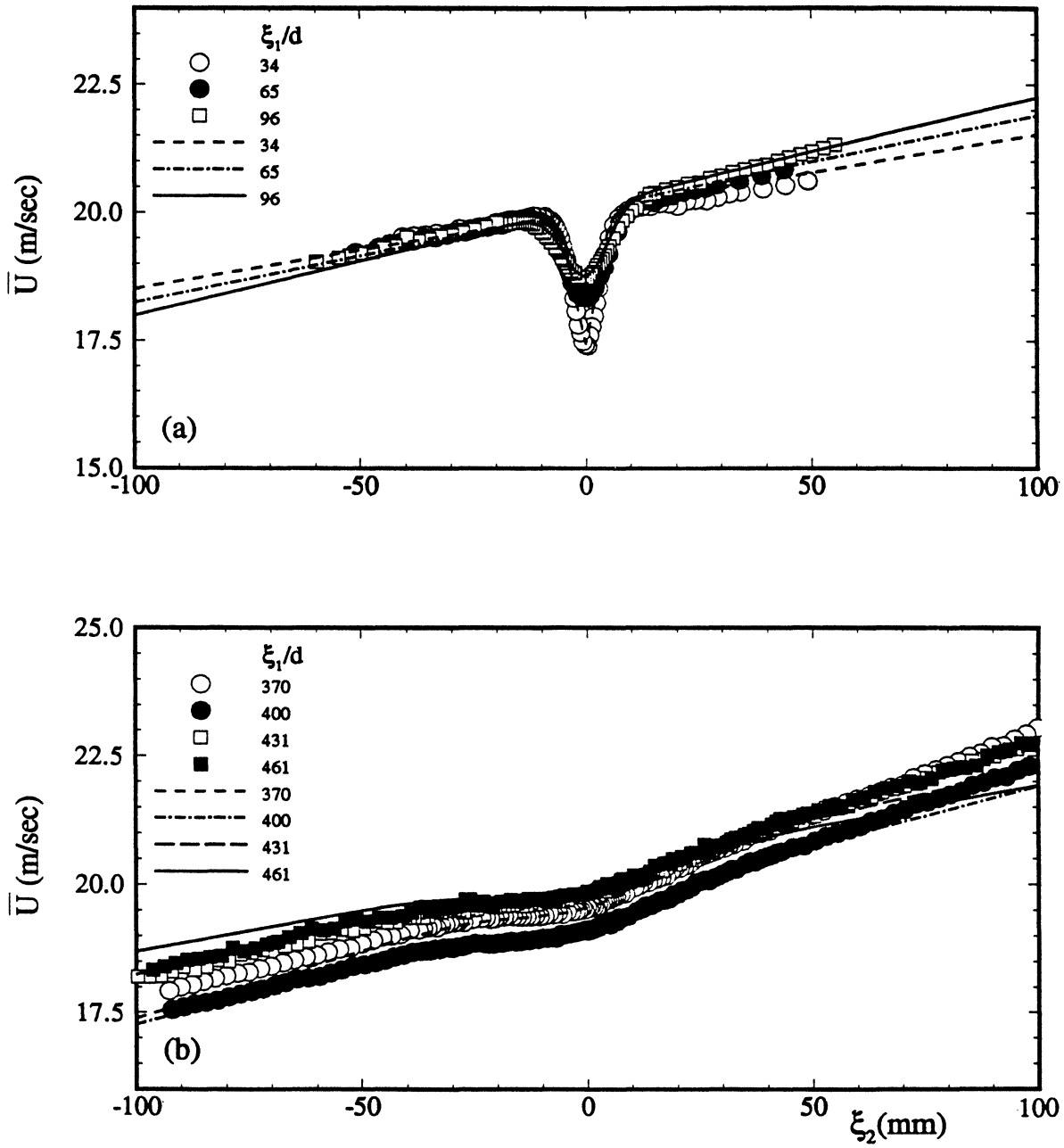

FIGURE 7 Mean longitudinal velocity distribution in curved channel, comparision of theory (lines) and experiment (symbols).

profiles are characterized by a highly dissipative vortical core inside the wake region surrounded by external potential flow region. A comparison with the developed theory shows a detailed prediction of this behavior over the entire velocity range confirming the validity of assumptions including the validity of the derived approximation for potential flow velocity in the vicinity of the wake center, i.e., $U_p = U_{p0}(1 - \frac{\xi_2}{R})$.

Reynolds stresses. The experimental results (symbols) for Reynolds shear stress distribution at various longitudinal locations are presented in Fig. 8 and are compared with the theory (lines) derived in Theoretical Consideration. The Reynolds shear stress is nondimensionalized by square of the maximum velocity defect. As shown in Fig. 8, unlike the straight channel case (Fig. 10), the curved channel shear stress is non-zero at the wake center

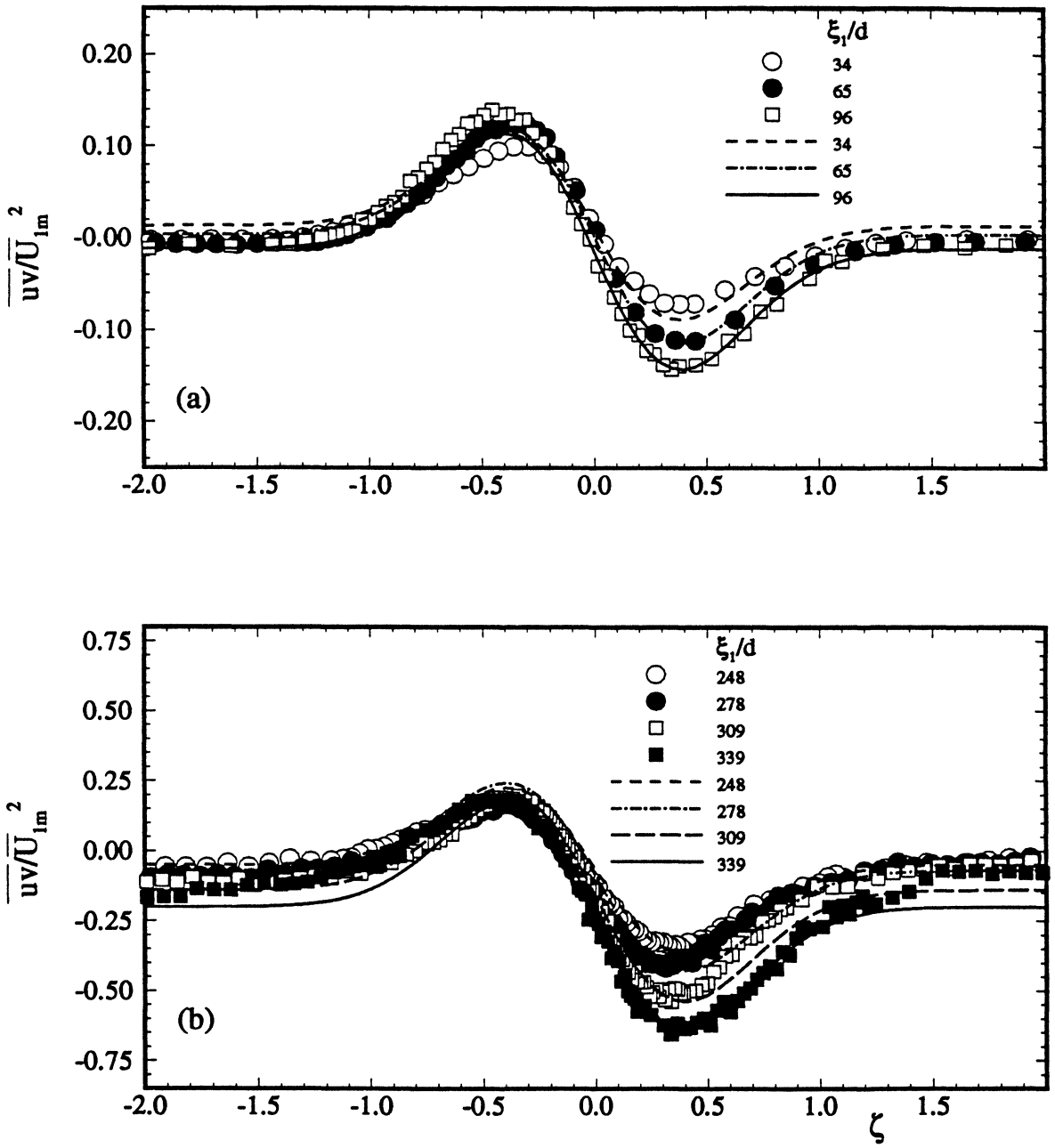

FIGURE 8 Reynolds shear stress distribution in curved channel, comparision of theory (lines) and experiment (symbols).

because of the curvature effect that causes a pressure gradient in lateral direction resulting in a highly asymmetric distribution of shear stress profiles. Raj and Lakshminarayana [1973] also observed non-zero value of Reynolds shear stress at the wake center. In their investigation, Raj and Lakshminarayana found that the point where $\partial \overline{U}/\partial y = 0$ (the wake center) need not to be the same where the Reynolds shear stress is zero. They concluded that the mixing length hypothesis is not valid for predicting the mean and turbulent quantities in such a region. For the present case it is observed to be located between convex wall and mean radius of the channel. The Reynolds shear stress in the hypothetical potential flow outside the wake is not exactly equal to zero due to the turbulence existing in that region with higher absolute value near the concave side of the wall ($\xi_2 < 0$).

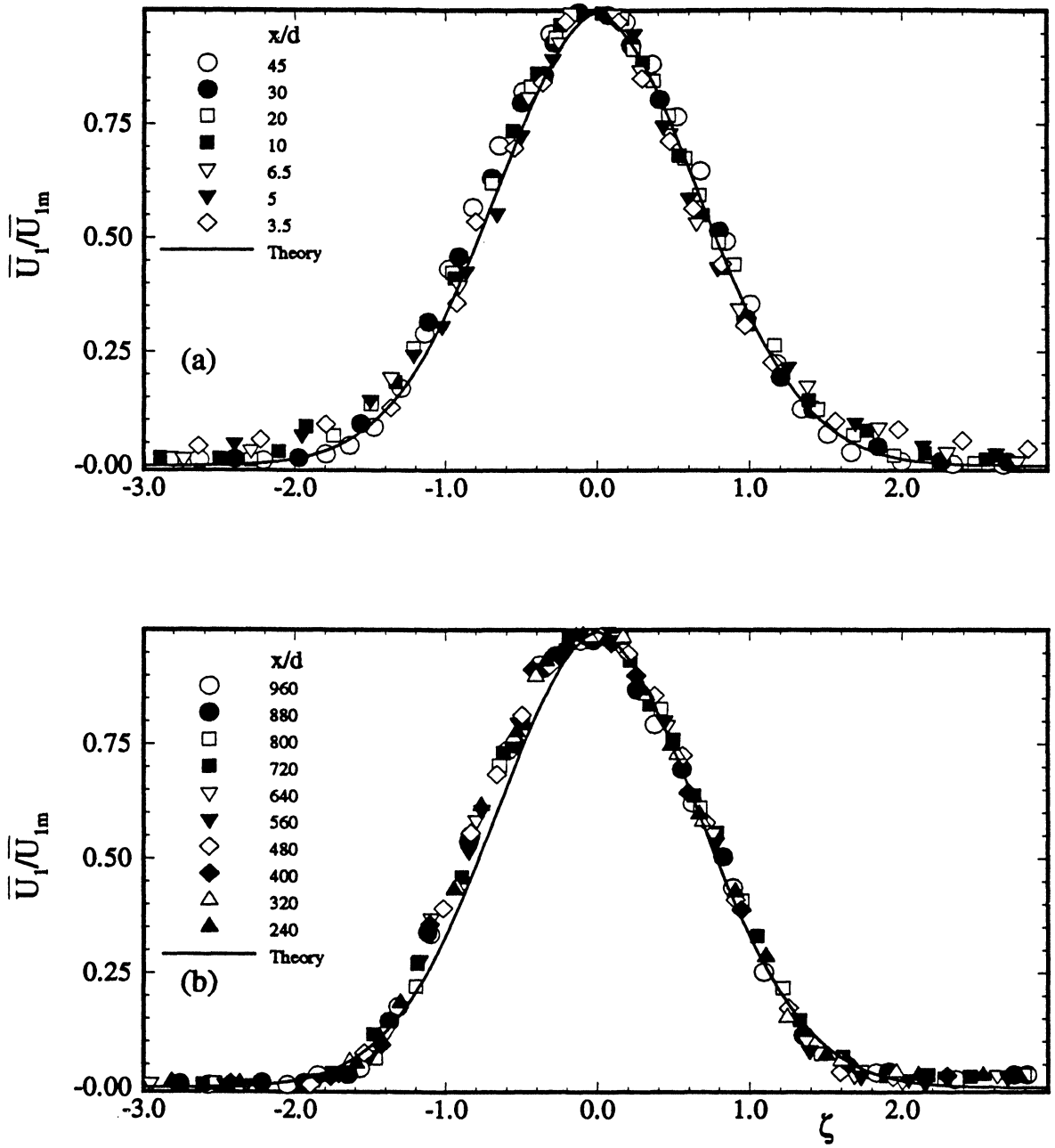

FIGURE 9 Mean defect velocity distribution in straight channel, theory (lines) compared with experimental data(symbols) from Eifler [1975]; (a) $d = 10$ mm; (b) $d = 0.5$ mm.

The experimentally determined shear stress distributions shown in Fig. 8(a, b) are compared with the developed theory. As described, the shear stress was calculated as the difference of the total impulse and the partial impulse $\overline{uv} = \overline{UV} - \overline{U}\,\overline{V}$ by integrating the conservation equations. The integration constants in the corresponding expressions were evaluated from experimental measurements corresponding to the values at the wake center. As can be seen from Fig. 8(a, b), the excellent agreement between the theory and the measurement over the entire range, particularly the precise prediction of the asymmetric pattern proves the validity of the assumptions necessary in developing the theoretical framework.

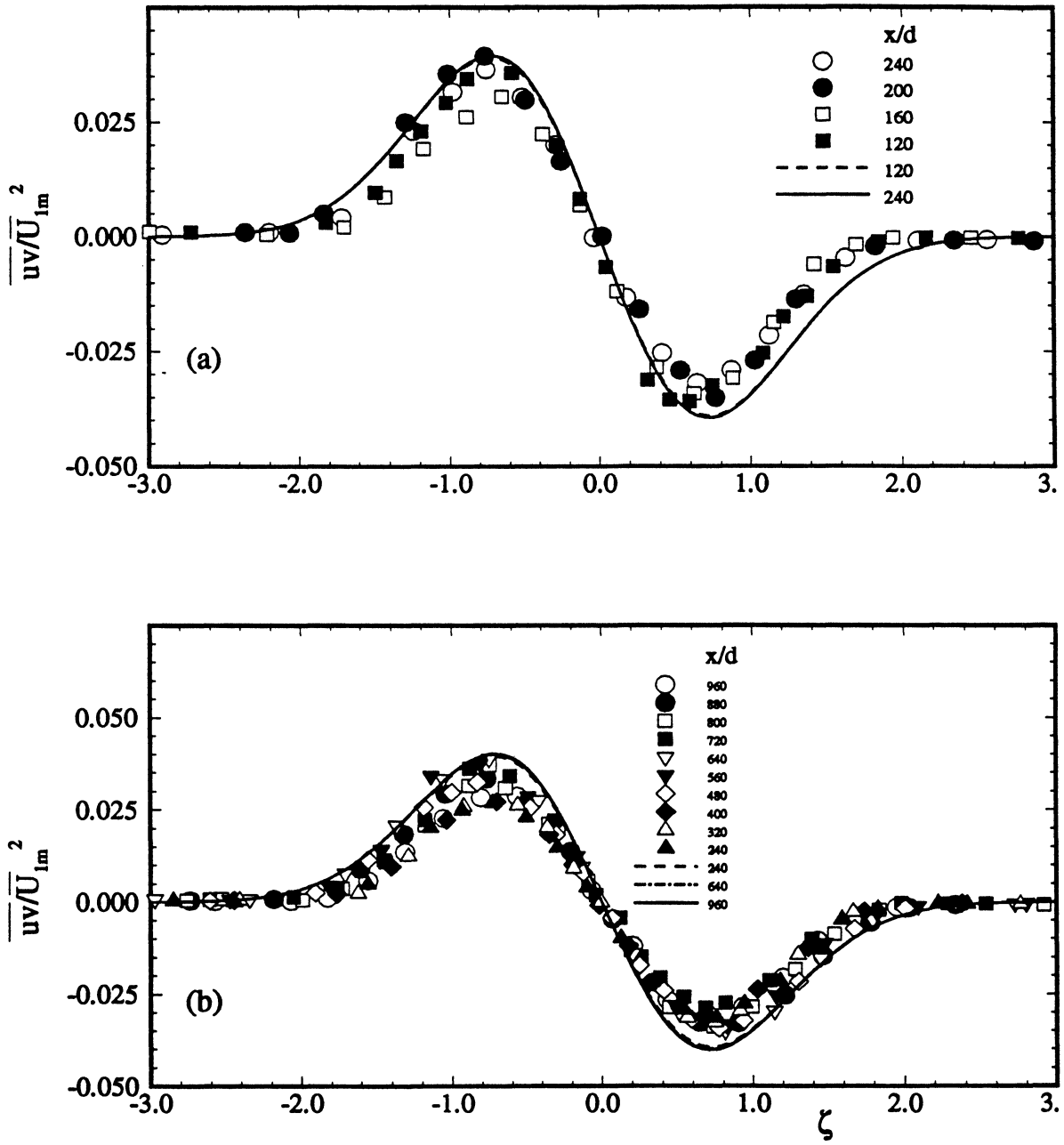

FIGURE 10 Reynolds shear stress distribution in straight channel, theory (lines) compared with experimental data (symbols) from Eifler [1975]; (a) $d = 1$ mm; (b) $d = 0.5$ mm.

Straight Channel Wake Flow

The developed theory, treats the straight channel wake flow as a classical special case in the sense that the radius of curvature approaches infinity. To demonstrate the general validity of the theoretical framework, it was found necessary to compare the theoretical results with the available experimental data from the literature. For this purpose, the experimental work by Eifler [1975] was chosen because it is probably the most comprehensive research work in this area and entails all the detailed information necessary for a theoretical evaluation and comparison. Eifler carried out experimental study of cylinder wake characteristics for a wide range of longitudinal locations and also for different diameters of cylinders in a straight channel.

The comparison of theory and experiment of mean wake velocity defect function for two different cylinder diameters $d = 10, 0.5$ mm at different longitudinal locations is presented in Fig. 9(a,b). As shown in Fig. 9, the wake development in longitudinal direction depends primarily upon the ratio x/d (ξ_1/d for curved wake) regardless of the separate variation of the parameters involved in this ratio. The excellent agreement of theory verifies the validity of the expression $\varphi_1 = e^{-\zeta^2}$. The same expression was found to predict both cases of straight and curved channel wake flows, provided that the wake velocity defect is defined properly.

Reynolds shear stress distributions for two different cylinder diameters $d = 1, 0.5$ mm at different longitudinal locations are shown in Fig. 10. The shear stress distribution is found to be symmetric about the wake center with a value of zero at the wake center making the integration constant in the expression for shear stress vanish. From the comparison, it is obvious that theory is in excellent agreement with measurement with the peaks being predicted quite reasonably.

CONCLUSIONS

The development of wake flow downstream of a cylindrical rod within a curved channel under zero longitudinal pressure gradient is experimentally investigated, compared with the theoretical framework developed, and presented in this paper. Mean and the turbulence quantities were measured and were transformed from the probe coordinate system into the curvilinear wake eigen-coordinate system. In contrast to the straight wake flow, the mean quantities of the curved wake including the longitudinal velocity component displayed an asymmetric pattern throughout the flow regime. The introduction of the velocity defect function and the wake width b as a single length scale resulted in a fully symmetric distribution of the nondimensionalized velocity defect $\varphi_1 = \overline{U}_1/\overline{U}_{1m} = f(\xi_2/b = \zeta)$. For the zero pressure gradient curved wake as well as straight wake, the experimental results have proved that the wake defect can be described by the function $\varphi_1 = e^{-\zeta^2}$. This function was implemented in the theory developed in Theoretical Considerations to calculate the total impulse $\overline{UV}$, the partial impulse $\overline{U}\,\overline{V}$, and the resulting shear stress $\overline{uv} = \overline{UV} - \overline{U}\,\overline{V}$. The experimental results were compared with the developed theory. It was shown that the new theoretical frame work is capable of predicting the zero-pressure gradient wake flow for both curved and straight channel boundary conditions. For validation of the theory, efforts are under way to prove the general validity of the theory using non-zero pressure gradient cases within an absolute frame of reference.

Nomenclature

b	wake width
c	integration constant
d	diameter of cylinder, the wake generating body
f	frequency
g_{ij}, g^{ij}	covariant and contravariant metric coefficients
N	total number of samples per channel of hot-film data for time averaging
r	radial position of probe from the center of the convex wall
r_i	radius of convex wall, $r_i = 500$ mm
R	radius of wake centerline
u	time-dependent physical component of velocity in longitudinal direction, ξ_1
$\overline{u^2}$	mean longitudinal turbulent fluctuation impulse
$\overline{uv}$	Reynolds shear stress
$\overline{U}$	time-averaged physical component of velocity in longitudinal direction
U_p	potential flow velocity in ξ_1 direction
$\overline{U}_1$	wake velocity defect, $\overline{U}_1 = U_p - \overline{U}$
$\overline{U}_{1m}$	maximum wake velocity defect
$\overline{U}_I^2$	wake momentum defect, $\overline{U}_I^2 = 2U_p\overline{U}_1 - \overline{U}_1^2$
$\overline{U}_{Im}^2$	maximum wake momentum defect
U_{p0}	hypothetical potential flow velocity at the wake center
$\overline{UV}$	total impulse
$\overline{U}\,\overline{V}$	partial impulse
v	time-dependent physical component of velocity in lateral direction, ξ_2
$\overline{v^2}$	mean lateral turbulent fluctuation impulse
$\underline{V}$	velocity vector
$\underline{\overline{V}}$	time-averaged mean velocity vector
$\underline{\tilde{V}}$	time-dependent fluctuating velocity vector
$\overline{V}$	time-averaged physical component of velocity in ξ_2 direction
V_x	velocity component along x-direction of probe coordinate system
V_y	velocity component along y-direction of probe coordinate system
V_{in}	average inlet velocity
V_{xp}	hypothetical potential velocity component along x-direction of probe
V^i	contravariant velocity component in ξ_i-direction

Greek letters

α	angle between resultant velocity vector and x-axis
Γ_{ij}^k	Christoffel symbols
ξ_1/d	measurement stations located downstream of wake
∇	$\vec{g}^i \frac{\partial}{\partial \xi_i}$, differential operator in ξ_i coordinate system
ξ_i	curvilinear coordinate system
ρ	density of air
ν	kinematic viscosity of air
ζ	dimensionless variable, $\zeta = \xi_2/b$
θ	angular position of the probe location from the inlet
ϑ	angle between probe and curvilinear coordinates
φ_1	dimensionless wake velocity defect
φ_2	dimensionless wake momentum defect

Subscripts, Superscripts

i, j, k tensor indices

References

Eifler, J., 1975. Zur Frage der freien turbulenten Strömungen, insbesondere hinter ruhenden und bewegten Zylindern, Dissertation D-17, Technische Hochschule Darmstadt, Germany.

John, J., and Schobeiri, T., 1993. A Simple and Accurate Method for Calibrating X-Probes, ASME Transactions, *Journal of Engineering Fluid Engineering,* Vol. **115,** pp. 148–152.

Lakshminarayana, B., and Raj, R., 1976. Three-Dimensional Characteristics of Turbulent Wakes Behind Rotors of Axial Flow Turbomachinery, ASME *Journal of Engineering for Power,* Vol. **98,** pp. 218–228.

Nakayama, A., 1987. Curvature and Pressure-Gradient Effects on a Small-Defect Wake, *Journal of Fluid Mechanics,* Vol. **175,** pp. 215–246.

Pfeil, H., and Eifler, J., 1975a. Zur Frage der Schubspannungsverteilung für die ebenen freien turbulenten Strömungen, *Forschung,* Ing.–Wes. 41, No. 4, pp. 105–112.

Pfeil, H., and Eifler, J., 1975b. Messungen im turbulenten Nachlauf des Einzelzylinders, *Forschung,* Ing.–Wes. 41, No. 5, pp. 137–145.

Reichardt, H., 1950. Gesetzmäßigkeiten der freien Turbulenz, VDI-Forsch.-Heft 414. 2. Auflage Düsseldorf, VDI-Verlag.

Raj, R., and Lakshminarayana, B., 1973. Characteristics of the Wake behind a Cascade of Airfoils, *Journal of Fluid Mechanics,* Vol. **81,** part 4, pp. 707–730.

Savill, A. M., 1983. The Turbulent Structure of a Highly Curved Two-Dimensional Wake, in *IUTAM Symposium on Complex Turbulent flows,* Eds. R. Dumas, and F. Fulachier, pp. 185–197. Marseille, Springer, Berlin: Heidelberg, New York.

Schobeiri, T., 1988. Establishment of a Research Facility for Investigating the Effects of Unsteady Inlet Flow Condition, Pressure Gradient and Curvature on Boundary Layer Transition and Heat Transfer, Internal Report, Texas A&M University, Turbomachinery Laboratory.

Schobeiri, T., and Pardivala, D., 1992. Development of a Subsonic Flow Research Facility for Simulating the Turbomachinery Flow and Investigating Its Effects on Boundary Layer Transition, Wake Development and Heat Transfer, *Proceedings of Fourth International Symposium on Transport Phenomena and Dynamics of Rotating Machinery,* pp. 98–114.